Article

Buffer-Assisted Proton-Coupled Electron Transfer in a Model Rhenium–Tyrosine Complex

Hiroshi Ishikita, Alexander V. Soudackov, and Sharon Hammes-Schiffer

J. Am. Chem. Soc., **2007**, 129 (36), 11146-11152• DOI: 10.1021/ja072708k • Publication Date (Web): 18 August 2007

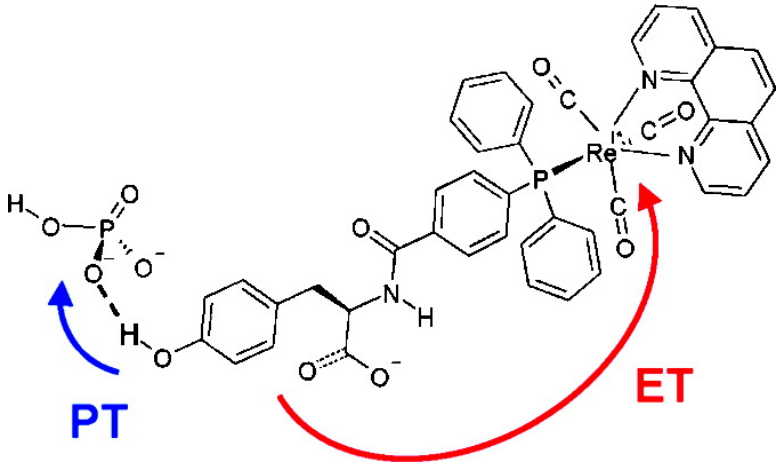

More About This Article

Additional resources and features associated with this article are available within the HTML version:

- Supporting Information
- Links to the 6 articles that cite this article, as of the time of this article download
- Access to high resolution figures
- Links to articles and content related to this article
- Copyright permission to reproduce figures and/or text from this article

View the Full Text HTML

J|A|C|S
ARTICLES
Published on Web 08/18/2007

Buffer-Assisted Proton-Coupled Electron Transfer in a Model Rhenium−Tyrosine Complex

Hiroshi Ishikita, Alexander V. Soudackov, and Sharon Hammes-Schiffer*

Contribution from the Department of Chemistry, 104 Chemistry Building, Pennsylvania State University, University Park, Pennsylvania 16802

Received April 18, 2007; E-mail: shs@chem.psu.edu

Abstract: The mechanism for tyrosyl radical generation in the $[Re(P-Y)(phen)(CO)_3]PF_6$ complex is investigated with a multistate continuum theory for proton-coupled electron transfer (PCET) reactions. Both water and the phosphate buffer are considered as potential proton acceptors. The calculations indicate that the model in which the proton acceptor is the phosphate buffer species HPO_4^{2-} can successfully reproduce the experimentally observed pH dependence of the overall rate and H/D kinetic isotope effect, whereas the model in which the proton acceptor is water is not physically reasonable for this system. The phosphate buffer species HPO_4^{2-} is favored over water as the proton acceptor in part because the proton donor−acceptor distance is ∼0.2 Å smaller for the phosphate acceptor due to its negative charge. The physical quantities impacting the overall rate constant, including the reorganization energies, reaction free energies, activation free energies, and vibronic couplings for the various pairs of reactant/product vibronic states, are analyzed for both hydrogen and deuterium transfer. The dominant contribution to the rate arises from nonadiabatic transitions between the ground reactant vibronic state and the third product vibronic state for hydrogen transfer and the fourth product vibronic state for deuterium transfer. These contributions dominate over contributions from lower product states because of the larger vibronic coupling, which arises from the greater overlap between the reactant and product vibrational wave functions. These calculations provide insight into the fundamental mechanism of tyrosyl radical generation, which plays an important role in a wide range of biologically important processes.

I. Introduction

Redox-active tyrosines play an important role in the proton-coupled electron transfer (PCET) reactions occurring in biological systems such as photosystem II (PSII) and class 1 ribonucleotide reductases (RNR). PSII possesses two redox-active tyrosines, Y_Z and Y_D, in the photosynthetic reaction center.[1] Following excitation of the primary electron donor P680, Y_Z is thought to mediate the PCET between the oxygen-evolving manganese−calcium cluster and P680.[2−6] Tyrosine radicals are also thought to be involved in the 35 Å PCET pathway of class 1 RNRs.[7] Understanding the fundamental mechanism of tyrosine oxidation[8−15] will assist in revealing the mechanisms of these biologically important processes.

In an effort to better understand these PCET mechanisms, tyrosine-bound ruthenium−tris-bipyridine model systems were synthesized and studied with the flash−quench method.[12−15] In these model systems, the excited state of Ru is quenched by an external quencher, methyl viologen, followed by electron transfer from the tyrosine to the photo-oxidized Ru and proton transfer from the tyrosine to the bulk solvent. Sjödin et al. explained the pH dependence of the experimentally measured PCET rate constant in the context of proton transfer from tyrosine to bulk water.[12−15] Subsequent theoretical calculations on this model system were consistent with this interpretation.[16] Alternative interpretations of this type of pH dependence have been proposed.[11,17]

To avoid the use of external quenchers, Reece and Nocera designed rhenium(I) polypyridyl complexes for the intramo-

(1) Loll, B.; Kern, J.; Saenger, W.; Zouni, A.; Biesiadka, J. *Nature* **2005**, *438*, 1040−1044.
(2) Groot, M. L.; Pawlowicz, N. P.; van Wilderen, L. J. G. W.; Breton, J.; van Stokkum, I. H. M.; van Grondelle, R. *Proc. Natl. Acad. Sci. U.S.A.* **2005**, *102*, 13087−13092.
(3) Tommos, C.; Tang, X.-S.; Warncke, K.; Hoganson, C. W.; Styring, S.; McCracken, J.; Diner, B. A.; Babcock, G. T. *J. Am. Chem. Soc.* **1995**, *117*, 10325−10335.
(4) Hoganson, C. W.; Babcock, G. T. *Science* **1997**, *277*, 1953−1956.
(5) Hoganson, C. W.; Lydakis-Simantiris, N.; Tang, X.-S.; Tommos, C.; Warncke, K.; Babcock, G. T.; Diner, B. A.; McCracken, J.; Styring, S. *Photosynth. Res.* **1995**, *47*, 177−184.
(6) Blomberg, M. R. A.; Siegbahn, P. E. M.; Styring, S.; Babcock, G. T.; Akermark, B.; Korall, P. *J. Am. Chem. Soc.* **1997**, *119*, 8285−8292.
(7) Stubbe, J.; Nocera, D. G.; Yee, C. S.; Chang, M. C. Y. *Chem. Rev.* **2003**, *103*, 2167−2202.
(8) Rhile, I. J.; Mayer, J. M. *J. Am. Chem. Soc.* **2004**, *126*, 12718−12719.
(9) Reece, S. Y.; Nocera, D. G. *J. Am. Chem. Soc.* **2005**, *127*, 9448−9458.
(10) Costentin, C.; Robert, M.; Saveant, J.-M. *J. Am. Chem. Soc.* **2006**, *128*, 4552−4553.
(11) Fecenko, C. J.; Meyer, T. J.; Thorp, H. H. *J. Am. Chem. Soc.* **2006**, *128*, 11020−11021.
(12) Sjodin, M.; Styring, S.; Akermark, B.; Sun, L.; Hammarstrom, L. *J. Am. Chem. Soc.* **2000**, *122*, 3932−3936.
(13) Sjodin, M.; Styring, S.; Akermark, B.; Sun, L.; Hammarstrom, L. *Philos. Trans. R. Soc. London B* **2002**, *357*, 1471−1479.
(14) Sjodin, M.; Ghanem, R.; Polivka, T.; Pan, J.; Styring, S.; Sun, L.; Sundstrom, V.; Hammarstrom, L. *Phys. Chem. Chem. Phys.* **2004**, *6*, 4851−4858.
(15) Sjodin, M.; Styring, S.; Wolpher, H.; Xu, Y.; Sun, L.; Hammarstrom, L. *J. Am. Chem. Soc.* **2005**, *127*, 3855−3863.
(16) Carra, C.; Iordanova, N.; Hammes-Schiffer, S. *J. Am. Chem. Soc.* **2003**, *125*, 10429−10436.
(17) Costentin, C.; Robert, M.; Saveant, J.-M. *J. Am. Chem. Soc.* **2007**, *129*, 5870−5879.

10.1021/ja072708k CCC: $37.00

lecular photogeneration of tyrosyl radical.[9] The specific complex of interest for the present paper is $[Re(P-Y)(phen)(CO)_3]PF_6$, where phen denotes 1,10-phenanthroline and P−Y denotes triphenylphosphine-tyrosine. For this system, tyrosine radicals can be produced directly from the metal-to-ligand charge-transfer (MLCT) excited state without an external quencher. Reece and Nocera analyzed the pH dependence of the rate constant for emission quenching in this complex.[9] At pH < 9, they observed that the rate constant increases with pH. This pH dependence of the rate constant for tyrosyl radical generation is consistent with a PCET mechanism. In principle, the proton acceptor for this reaction could be either water or the phosphate buffer. Recent experiments indicate that the phosphate buffer species HPO_4^{2-} is the proton acceptor.[18,19]

In this paper, we investigate the detailed mechanism for tyrosyl radical generation in the $[Re(P-Y)(phen)(CO)_3]PF_6$ system with a multistate continuum theory for PCET reactions.[20−22] We test both water and phosphate as potential proton acceptors and determine that only the phosphate-acceptor model is consistent with the experimental data. We also analyze the mechanism to elucidate the various contributions to the rate, including the reorganization energies, reaction free energies, activation free energies, and vibronic couplings for the various pairs of reactant/product vibronic states for both hydrogen and deuterium transfer. Section II describes the theoretical formulation and the computational methodology, section III presents the results and analysis, and section IV summarizes the conclusions of this study.

II. Theory and Methods

A. General Theoretical Formulation. A variety of theoretical approaches for the description of PCET reactions have been developed.[20−26] The present study is based on the multistate continuum theory for PCET reactions.[20−22] We investigate the PCET reaction in the system depicted in Figure 1 and the related reaction in which the proton transfers directly to bulk water. For these reactions, the electron donor is tyrosine (YOH), the electron acceptor is Re^{I*}, the proton donor is YOH, and the proton acceptor is either HPO_4^{2-} in the phosphate-acceptor model or bulk water in the water-acceptor model. Our calculations focus on the PCET reaction in water with pH = 5−9, so the tyrosine can be assumed to be initially protonated because the pK_a of tyrosine is 10.[27] In this case, the PCET reaction can be described in terms of the following four diabatic states:

$$\begin{aligned} &(1a) && Re^{I*}-YOH\cdots A_p \\ &(1b) && Re^{I*}-YO^{-}\cdots {}^{+}HA_p \\ &(2a) && Re^{0}-YOH^{\bullet +}\cdots A_p \\ &(2b) && Re^{0}-YO^{\bullet}\cdots {}^{+}HA_p \end{aligned} \qquad (1)$$

where 1 and 2 denote the electron-transfer (ET) state, and *a* and *b* denote the proton-transfer (PT) state. Within this notation, $1a \rightarrow 1b$ represents PT, $1a \rightarrow 2a$ represents ET, and $1a \rightarrow 2b$ represents EPT, where the proton and the electron are transferred simultaneously. Here, A_p represents a general proton acceptor.

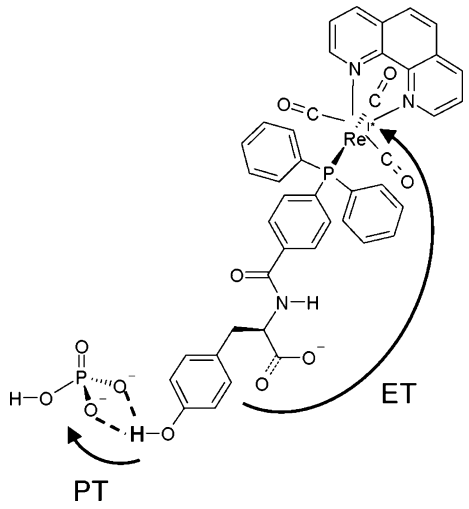

Figure 1. Structure of the rhenium−tyrosine complex[9] hydrogen-bonded to a phosphate HPO_4^{2-} acceptor. The proton transfer and electron transfer reactions are indicated with arrows. The net charge of ReYOH is zero, and the overall charge of the entire hydrogen-bonded complex is 2−.

In the multistate continuum theory for PCET,[20−22] the free energy surfaces are calculated as functions of two collective solvent coordinates, z_p and z_e, corresponding to PT and ET, respectively. When the PT reaction is electronically adiabatic and the ET/EPT reactions are electronically non-adiabatic, the diabatic free energy surfaces corresponding to ET states 1 and 2 are calculated as mixtures of the *a* and *b* PT states. In this case, the reactants (I) are mixtures of the 1*a* and 1*b* states, and the products (II) are mixtures of the 2*a* and 2*b* states. The proton vibrational states are calculated for both the reactant (I) and product (II) diabatic surfaces, leading to two sets of two-dimensional vibronic free energy surfaces. The PCET reaction is described in terms of nonadiabatic transitions from the reactant (I) to the product (II) PCET vibronic states. In this paper, EPT refers to the transfer of an electron and a proton between pure diabatic states (i.e., $1a \rightarrow 2b$), while PCET refers to the overall reaction from reactant (I) to product (II) diabatic surfaces.

Within this framework, the unimolecular rate expression for PCET is[21]

$$k_{PCET}^{uni} = \frac{2\pi}{\hbar}\sum_{\mu} P_{I\mu}\sum_{\nu}|V_{\mu\nu}|^2(4\pi\lambda_{\mu\nu}k_BT)^{-1/2}\exp\left(\frac{-\Delta G_{\mu\nu}^{\dagger}}{k_BT}\right) \qquad (2)$$

where $\sum_\mu$ and $\sum_\nu$ indicate summations over reactant and product PCET vibronic states, respectively, and $P_{I\mu}$ is the Boltzmann factor for reactant state $I\mu$. The free energy barrier is

$$\Delta G_{\mu\nu}^{\dagger} = \frac{(\Delta G_{\mu\nu}^{o} + \lambda_{\mu\nu})^2}{4\lambda_{\mu\nu}} \qquad (3)$$

where the free energy difference is defined as

$$\Delta G_{\mu\nu}^{o} = \epsilon_{\nu}^{II}(\bar{z}_p^{II\nu},\bar{z}_e^{II\nu}) - \epsilon_{\mu}^{I}(\bar{z}_p^{I\mu},\bar{z}_e^{I\mu}) \qquad (4)$$

Here, $(\bar{z}_p^{I\mu},\bar{z}_e^{I\mu})$ and $(\bar{z}_p^{II\nu},\bar{z}_e^{II\nu})$ are the solvent coordinates for the minima of the ET diabatic free energy surfaces $\epsilon_\mu^I(z_p,z_e)$ and $\epsilon_\nu^{II}(z_p,z_e)$, respectively. In the high-temperature approximation for uncoupled solute

(18) Reece, S. Y.; Nocera, D. G., personal communication.
(19) Irebo, T.; Reece, S. Y.; Sjodin, M.; Nocera, D. G.; Hammarstrom, L. *J. Am. Chem. Soc.*, submitted.
(20) Soudackov, A.; Hammes-Schiffer, S. *J. Chem. Phys.* **1999**, *111*, 4672−4687.
(21) Soudackov, A.; Hammes-Schiffer, S. *J. Chem. Phys.* **2000**, *113*, 2385−2396.
(22) Hammes-Schiffer, S. *Acc. Chem. Res.* **2001**, *34*, 273−281.
(23) Cukier, R. I. *J. Phys. Chem.* **1996**, *100*, 15428−15443.
(24) Cukier, R. I.; Nocera, D. G. *Annu. Rev. Phys. Chem.* **1998**, *49*, 337−369.
(25) Mayer, J. M.; Hrovat, D. A.; Thomas, J. L.; Borden, W. T. *J. Am. Chem. Soc.* **2002**, *124*, 11142−11147.
(26) Georgievskii, Y.; Stuchebrukhov, A. A. *J. Chem. Phys.* **2000**, *113*, 10438−10450.
(27) Dixon, W. T.; Murphy, D. *J. Chem. Soc., Faraday Trans. 2* **1976**, *72*, 1221−1230.

modes, the total reorganization energy is expressed as the sum of the outer-sphere (solvent) and inner-sphere (solute) contributions:[21,2828]

$$\lambda_{\mu\nu} = (\lambda_o)_{\mu\nu} + \lambda_{in} \quad (5)$$

The outer-sphere reorganization energy is defined as

$$(\lambda_o)_{\mu\nu} = \epsilon_\mu^I(\bar{z}_p^{II\nu},\bar{z}_e^{II\nu}) - \epsilon_\mu^I(\bar{z}_p^{I\mu},\bar{z}_e^{I\mu}) = \epsilon_\nu^{II}(\bar{z}_p^{I\mu},\bar{z}_e^{I\mu}) - \epsilon_\nu^{II}(\bar{z}_p^{II\nu},\bar{z}_e^{II\nu}) \quad (6)$$

and the inner-sphere reorganization energy λ_{in} can be estimated from electronic structure calculations or experimental data. The coupling $V_{\mu\nu}$ in the PCET rate expression is defined as

$$V_{\mu\nu} = \langle \phi_\mu^I | V(r_p, z_p^\dagger) | \phi_\nu^{II} \rangle_p \quad (7)$$

where the subscript of the angular brackets indicates integration over the proton coordinate r_p, $z_p^\dagger$ is the value of z_p in the intersection region, and ϕ_μ^I and ϕ_ν^{II} are the proton vibrational wave functions for the reactant and product ET diabatic states, respectively. The electronic coupling $V(r_p,z_p^\dagger)$ between the reactant (I) and product (II) diabatic surfaces is expressed in terms of the diagonal and off-diagonal matrix elements of a 4×4 empirical valence bond (EVB) Hamiltonian in the complex way described by eqs 16−22 in ref 21.

B. Calculation of Input Quantities. 1. Atomic Coordinates and Charges. The atomic coordinates for the PCET complex are required for the calculation of the outer-sphere reorganization energies. Our model of the atomic coordinates for the ReYOH complex depicted in Figure 1 is based on the crystal structure of a similar complex, [Re(phenanthroline)(bis-diphenylphospinoethylene)$(CO)_2$]](PF_6).[9] Initially, we used GaussView 3.0[29] to modify this crystal structure to represent the ReYOH complex being studied. Subsequently, we optimized the geometry of the ReYOH complex with density functional theory (DFT) at the B3LYP/LACV3P** level.[30−32] These calculations were performed with the JAGUAR program.[33] The geometry optimization was performed for the ground state, Re^I(YOH), corresponding to the situation prior to photoexcitation. Nuclear rearrangements upon photoexcitation will not significantly impact the calculated outer-sphere reorganization energies, which are affected by the changes in solute charge distribution upon charge transfer. Moreover, the tyrosine carboxylic acid was protonated during the gas-phase geometry optimization to avoid non-physical electrostatic interactions between the carboxylate group and the rhenium. As discussed below, the carboxylic acid was deprotonated during the calculation of the outer-sphere reorganization energies. We also optimized the geometries for the hydrogen-bonded complexes comprised of tyrosine (i.e., methyl phenol) with a phosphate molecule (HPO_4^{2-}) and tyrosine with three water molecules using DFT at the B3LYP/6-31G** level with the polarized continuum model.[34] These calculations were performed with Gaussian03.[35] The complete ReYOH complex, hydrogen-bonded to a phosphate molecule or three water molecules, was obtained by superimposing the tyrosine aromatic rings from the ReYOH and the tyrosine−proton-acceptor geometry optimizations. The atomic coordinates are provided in Table S1 in the Supporting Information.

The atomic charges are also required for the calculation of the outer-sphere reorganization energies. The tyrosine carboxylic acid was deprotonated for all of these calculations since we are studying the reaction for pH > 5.[9] Subsequent to photoexcitation, Re is in the electronically excited Re^{I*} state before ET and in the Re^0 state after ET. Although DFT studies imply that the orbital in the excited state may have CO ligand character,[36] we represent the Re^{I*} state as Re^{2+}(phenanthroline)$^-$ and the Re^0 state as Re^+(phenanthroline)$^-$ for these calculations. Thus, the phenanthroline ligand is always negatively charged in the present study. The atomic charges on the protonated and deprotonated tyrosine, the (phenanthroline)$^-$ and triphenylphosphine ligands, H_2O, H_3O^+, HPO_4^{2-}, and $H_2PO_4^-$ were obtained by optimizing the isolated ligands with DFT at the B3LYP/6-31G** level and subsequently applying the CHELPG method[37] to the optimized ligands. The atomic charges on the peptide backbone and the CO ligands were adopted from the all-atom CHARMM22 parameter set.[38] The atomic charges used for the calculation of the outer-sphere reorganization energies are provided in Table S2 in the Supporting Information.

2. Reorganization Energies. The outer-sphere (solvent) reorganization energies are calculated with the frequency-resolved cavity model.[39,40] The two effective radii for the solute atoms are defined as $r_\infty = \kappa r_{vdW}$ and $r_{in} = r_\infty + \delta$, where r_{vdW} is the van der Waals radius, κ is a universal scaling factor, and δ is a constant specific to the particular solvent. We used $\kappa = 0.9$ and $\delta = 0.9$ and the static and optical dielectric constants of $\epsilon_o = 78.4$ and $\epsilon_\infty = 1.78$ for water at 298 K, as used in previous applications.[16] All atoms of the complex are included for the calculation of the solvent reorganization energies, with the atomic coordinates and charges provided in Tables S1 and S2. Note that the atomic charges for the 2*a* diabatic state were obtained as a function of the atomic charges in the other three diabatic states (i.e., $q_{2a} = q_{2b} - q_{1b} + q_{1a}$, where q_i is the charge on each atom in diabatic state i) to maintain consistent charge densities within the valence bond (VB) theory.[20]

The calculation of the inner-sphere reorganization energy requires geometry optimizations of the Re^{I*} and Re^0 excited states of the ReYOH complex. The accurate calculation of these geometries with currently available electronic structure methods is extremely challenging. Thus, we estimate the inner-sphere reorganization energy from the approximate total reorganization energy of 1.9 eV observed experimentally for related systems.[41,42] Specifically, the inner-sphere reorganization energy is estimated as the difference between this total reorganization energy and the calculated outer-sphere reorganization energy for electron transfer in these systems. According to this prescription, the inner-sphere reorganization energy is estimated to be 9.8 kcal/mol. We found that the overall results do not change qualitatively when the inner-sphere reorganization energy is set to zero, as long as the couplings V^{PT} and V^{ET} are decreased accordingly. The sensitivity of the results to inner-sphere reorganization energy is illustrated in the Supporting Information.

3. Gas Phase Potential. The gas phase EVB Hamiltonian matrix elements for the PCET reaction are based on a linear, five-site model:

$$O_{acceptor}-H-O_{tyrosine}-Y-Re$$

where $O_{acceptor}$ is the proton acceptor, $O_{tyrosine}$ is the proton donor, Y is the electron donor, and Re is the electron acceptor. The distances within

(28) Iordanova, N.; Decornez, H.; Hammes-Schiffer, S. *J. Am. Chem. Soc.* **2001**, *123*, 3723−3733.
(29) Dennington, R., II; Keith, T.; Millam, J. M.; Eppinnett, K.; Hovell, W. L.; Gilliland, R. *GaussView*, Version 3.0; Semichem, Inc.: Shawnee Mission, KS, 2003.
(30) Ditchfield, R.; Hehre, W. J.; Pople, J. A. *J. Chem. Phys.* **1971**, *54*, 724−728.
(31) Hehre, W. J.; Ditchfield, R.; Pople, J. A. *J. Chem. Phys.* **1972**, *56*, 2257−2261.
(32) Francl, M. M.; Pietro, W. J.; Hehre, W. J.; Binkley, J. S.; Gordon, M. S.; DeFrees, D. J.; Pople, J. A. *J. Chem. Phys.* **1982**, *77*, 3654−3665.
(33) *Jaguar*, 6.0; Schrodinger, Inc.: Portland, OR, 2005.
(34) Miertus, S.; Scrocco, E.; Tomasi, J. *Chem. Phys.* **1981**, *55*, 117−129.
(35) Frisch, M. J.; et al. *Gaussian 03*, revision C.03; Gaussian, Inc.: Pittsburgh, PA, 2003.
(36) Dattelbaum, D. M.; Omberg, K. M.; Schoonover, J. R.; Martin, R. L.; Meyer, T. J. *Inorg. Chem.* **2002**, *41*, 6071−6079.
(37) Breneman, C. M.; Wiberg, K. B. *J. Comput. Chem.* **1990**, *11*, 361−373.
(38) Brooks, B. R.; Bruccoleri, R. E.; Olafson, B. D.; States, D. J.; Swaminathan, S.; Karplus, M. *J. Comput. Chem.* **1983**, *4*, 187−217.
(39) Basilevsky, M. V.; Rostov, I. V.; Newton, M. D. *Chem. Phys.* **1998**, *232*, 189−199.
(40) Newton, M. D.; Basilevsky, M. V.; Rostov, I. V. *Chem. Phys.* **1998**, *232*, 201−210.
(41) Reece, S. Y.; Seyedsayamdost, M. R.; Stubbe, J.; Nocera, D. G. *J. Am. Chem. Soc.* **2006**, *128*, 13654−13655.
(42) In ref 41, the total reorganization energy is estimated experimentally to be 1.9 eV for electron transfer in a series of $[Re(bpy)(CO)_3CN]-F_nY^-$ complexes. Consistent values were obtained from the experimentally observed dependence of the electron-transfer rates on the driving force and on temperature using a non-adiabatic Marcus theory formalism.

this five-site model were obtained from the geometry optimizations of the hydrogen-bonded ReYOH−A_p complexes: the electron donor was chosen to be the center of the tyrosine ring, the proton donor was chosen to be the oxygen atom on the tyrosine, the electron acceptor was chosen to be the rhenium, and the proton acceptor was chosen to be the relevant oxygen atom on the phosphate or water molecule.

The diagonal matrix elements for this system are expressed as

$$\begin{aligned}(h_o)_{1a,1a} &= U^{\text{Morse}}_{O_DH} + U^{\text{rep}}_{O_AH}\\ (h_o)_{1b,1b} &= U^{\text{Morse}}_{O_AH} + U^{\text{rep}}_{O_DH} + \Delta E_{1b}\\ (h_o)_{2a,2a} &= U^{\text{Morse}}_{O_DH} + U^{\text{rep}}_{O_AH} + \Delta E_{2a}\\ (ho)_{2b,2b} &= U^{\text{Morse}}_{O_AH} + U^{\text{rep}}_{O_DH} + \Delta E_{2b}\end{aligned} \tag{8}$$

where U^{Morse} and U^{rep} denote the Morse potential for the O−H bond and the repulsion term between nonbonded O and H atoms. Here, ΔE denotes the energy difference of each diabatic state relative to the diabatic state 1*a* and is adjusted to reproduce the driving forces for PT, ET, and EPT. The Morse potential for an O−H bond of length R_{OH} is

$$U^{\text{Morse}}_{OH} = D_{OH}(1 - e^{-\beta_{OH}(R_{OH}-R^o_{OH})})^2 \tag{9}$$

where $D_{OH} = 102$ kcal/mol and $R^o_{OH} = 0.96$ Å based on typical O−H bonds.[43] In addition, $\beta_{OH} = 2.35$ Å^{-1}, corresponding to ∼3630−3660 cm^{-1} for tyrosine,[43,44] $\beta_{OH} = 1.67$ Å^{-1}, corresponding to ∼2580 cm^{-1} for oxidized cationic tyrosine, $\beta_{OH} = 1.73$ Å^{-1}, corresponding to ∼2670 cm^{-1} for H_3O^+,[45] and $\beta_{OH} = 1.85$ Å^{-1}, corresponding to ∼2850−2950 cm^{-1} for $H_2PO_4^-$.[46,47] The repulsion term between nonbonded atoms O and H separated by distance R_{OH} is

$$U^{\text{rep}}_{OH} = D'_{OH}\, e^{-\beta'_{OH}R_{OH}} \tag{10}$$

where $\beta'_{OH} = 2.5$ Å^{-1} and $D'_{OH} = 500$ (1000) kcal/mol for tyrosine (water), as used in previous applications for a similar system.[16] The results do not change qualitatively when these gas phase parameters are modified within physically reasonable ranges.

As in previous studies,[16] the couplings between the diabatic states are assumed to be constant:

$$\begin{aligned}(h_o)_{1a,1b} &= (h_o)_{2a,2b} = V^{\text{PT}}\\ (h_o)_{1a,2a} &= (h_o)_{1b,2b} = V^{\text{ET}}\\ (h_o)_{1a,2b} &= (h_o)_{1b,2a} = V^{\text{EPT}}\end{aligned} \tag{11}$$

In the phosphate-acceptor model, we used coupling constants $V^{\text{ET}} = 0.14668$ kcal/mol and $V^{\text{PT}} = 34.29$ kcal/mol. The basis for choosing these values is discussed below. Within VB theory, V^{EPT} is expected to be significantly smaller than V^{ET}, so we chose $V^{\text{EPT}} = 0$ for simplicity.

4. Driving Forces. The quantities ΔE in the diagonal matrix elements are determined by reproducing the driving forces for PT, ET, and EPT. This subsection describes the calculation of estimates for these driving forces (i.e., reaction free energies). The thermodynamic cycle for the four diabatic states in the phosphate-acceptor model is summarized in Figure 2. The driving forces are calculated for the diabatic states, and

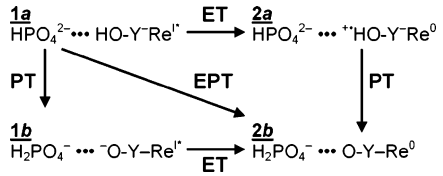

Figure 2. Thermodynamic cycle for the four diabatic states in the phosphate-acceptor model.

the ReYOH complex and proton acceptor are assumed to be infinitely separated with no hydrogen bonding for the diabatic states. In all cases, the calculations rely on significant approximations and should be considered to be only estimates of the actual values.

For both models, the electron donor is YOH and the electron acceptor is Re^{I*}. The corresponding ET reaction is

$$\text{YOH} + \text{Re}^{\text{I}*} \rightarrow \text{YOH}^{\bullet+} + \text{Re}^0 \tag{12}$$

The driving force for this ET reaction is the difference between the reduction potentials for YOH and Re^{I*}. A pH-independent value of $E^o(\text{YOH}^{\bullet+}/\text{YOH}) = +1.38$ V has been estimated from experimental data,[48] and the reduction potential $E^o(\text{Re}^{\text{I}*/0})$ has been experimentally measured to be +1.78 V.[9] Thus, the reaction free energy for ET can be expressed as

$$\begin{aligned}\Delta G^o_{1a\rightarrow 2a} &= -23.061 \text{ kcal/mol V}^{-1}\\ &\quad [E^o(\text{Re}^{\text{I}*/0}) - E^o(\text{YOH}^{\bullet+}/\text{YOH})]\\ &= -9.22 \text{ kcal/mol}\end{aligned} \tag{13}$$

The driving forces for PT and EPT differ for the phosphate-acceptor and water-acceptor models. For both models, the calculation of these driving forces uses the experimental pK_a values for tyrosine,[27] $pK_a(\text{YOH}/\text{YO}^-) = 10$ and $pK_a(\text{YOH}^{\bullet+}/\text{YO}^{\bullet}) = -2$. For the phosphate-acceptor model, the calculation also requires the experimental pK_a value for phosphate,[49,50] $pK_a(H_2PO_4^-/HPO_4^{2-}) = 7.2$.

In the phosphate-acceptor model, the proton donor is YOH and the proton acceptor is HPO_4^{2-}. In this case, the PT reaction is

$$\text{YOH} + \text{HPO}_4^{2-} \rightarrow \text{YO}^- + \text{H}_2\text{PO}_4^- \tag{14}$$

The reaction free energy for this PT reaction is

$$\begin{aligned}\Delta G^o_{1a\rightarrow 1b} &= 1.368 \text{ kcal/mol}\\ &\quad [pK_a(\text{YOH}/\text{YO}^-) - pK_a(H_2PO_4^-/HPO_4^{2-})]\\ &= 3.830 \text{ kcal/mol}\end{aligned} \tag{15}$$

The EPT reaction for this model is

$$\text{Re}^{\text{I}*} + \text{YOH} + \text{HPO}_4^{2-} \rightarrow \text{YO}^{\bullet} + \text{H}_2\text{PO}_4^- + \text{Re}^0 \tag{16}$$

The reaction free energy for the EPT reaction can be expressed as

$$\begin{aligned}\Delta G^o_{1a\rightarrow 2b} &= -23.061 \text{ kcal/mol V}^{-1}\\ &\quad [E^o(\text{Re}^{\text{I}*/0}) - E^o(\text{YOH}^{\bullet+}/\text{YOH})]\\ &\quad + 1.368 \text{ kcal/mol}\\ &\quad [pK_a(\text{YOH}^{\bullet+}/\text{YO}^{\bullet}) - pK_a(H_2PO_4^-/HPO_4^{2-})]\\ &= -21.8 \text{ kcal/mol}\end{aligned} \tag{17}$$

In D_2O, experimental measurements indicate that $pK_a(D_2PO_4^-/DPO_4^{2-})$

(43) Warshel, A. *Computer Modeling of Chemical Reactions in Enzymes and Solutions*; John Wiley & Sons, Inc.: New York, 1991.
(44) Fujii, A.; Ebata, T.; Mikami, N. *J. Phys. Chem. A* **2002**, *106*, 8554−8560.
(45) Okamura, M.; Yeh, L. I.; Myers, J. D.; Lee, Y. T. *J. Phys. Chem.* **1990**, *94*, 3416−3427.
(46) Gerhards, M.; Jansen, A.; Unterberg, C.; Kleinermanns, K. *Chem. Phys. Lett.* **2001**, *344*, 113−119.
(47) Kleinermanns, K.; Janzen, C.; Spangenberg, D.; Gerhards, M. *J. Phys. Chem. A* **1999**, *103*, 5232−5239.
(48) Tommos, C.; Babcock, G. T. *Biochim. Biophys. Acta* **2000**, *1458*, 199−219.
(49) Sorensen, S. P. L. *Biochem Z.* **1909**, *21*, 131−304.
(50) Sorensen, S. P. L. *Biochem. Z.* **1909**, *22*, 352−356.

Table 1. Calculated Diabatic Solvent Reorganization Energies for the ReYOH Complex Hydrogen-Bonded to the Proton Acceptor

	reorganization energy (kcal/mol)		
proton acceptor	ET	PT	EPT
HPO_4^{2-}	33.9	8.03	34.8
H_2O	33.7	8.40	38.7

$= 7.8$[51] and $pK_a(YOD/YO^-) = 10.6$.[18] Since these pK_a shifts are the same, the driving force is expected to be the same for proton and deuteron transfer from tyrosine to phosphate.

For the water-acceptor model, the proton donor is YOH and the proton acceptor is bulk water. In this case, the pH dependence of the reaction can be incorporated into the driving forces for PT and EPT in a phenomenological manner.[12,16] We emphasize that this procedure is not rigorous and only phenomenologically incorporates the macroscopic properties of bulk water through the pH dependence of these driving forces. As will be shown below, the water-acceptor model does not reproduce the experimental data. Thus, this procedure involving pH-dependent driving forces does not provide an even qualitatively correct description of this PCET reaction and is not used in the final analysis. Alternative theoretical descriptions of these types of PCET reactions[17] could also be applied to this system, but such studies are beyond the scope of this work.

5. Sensitivity of Results to Parameters. In this subsection, we summarize the dependence of the results on the various parameters in the model. The parameters in the gas phase potential are determined from gas phase quantum mechanical calculations and experimental bond lengths, dissociation energies, and frequencies. The parameters corresponding to the driving forces are estimated from the experimental pK_a and redox potential values. The outer-sphere reorganization energies are calculated with dielectric continuum models, and the inner-sphere reorganization energy is estimated from experimental studies on related systems. The results are not sensitive to the variation of any of these parameters within physically reasonable ranges.

The only parameters that are fit directly to the kinetic data are V^{ET}, which impacts mainly the magnitude of the rate, and V^{PT}, which determines the proton-transfer barrier and therefore impacts both the magnitude of the rate and the kinetic isotope effect (KIE). The sensitivity of the calculated KIE to the V^{PT} coupling parameter and to the inner-sphere reorganization energy λ_{in} for the phosphate-acceptor model is illustrated in the Supporting Information. We have found that the experimentally observed KIE can be reproduced with reasonable values of V^{PT} in the relatively narrow range of 25−35 kcal/mol for this model.

III. Results and Discussion

The diabatic solvent reorganization energies are given in Table 1. The solvent reorganization energies for PT are significantly smaller than those for ET and EPT because the proton is transferred over a much smaller distance than the electron. The solvent reorganization energies for EPT are slightly greater than those for ET because the electron and proton are transferring in opposite directions, leading to a greater charge separation for EPT than for ET. The ET solvent reorganization energies are identical for the water-acceptor and phosphate-acceptor models, but the PT and EPT solvent reorganization energies are slightly smaller for the phosphate-acceptor model than for the water-acceptor model, due mainly to the larger size of the phosphate molecule, resulting in greater solvent exclusion.

For the phosphate-acceptor model, the pH dependence of the overall rate is assumed to arise from the titration between the HPO_4^{2-} and $H_2PO_4^-$ forms of the phosphate buffer. The proton is assumed to transfer to HPO_4^{2-} but not to $H_2PO_4^-$. These assumptions are consistent with the experimental observations that the rate constant is independent of pH for $4 < pH < 8$ in the absence of the phosphate buffer and that the dependence of the rate on phosphate buffer concentration is absent at low pH, where the dominant buffer species is $H_2PO_4^-$.[18] Given these assumptions, the overall rate constant for tyrosine oxidation can be expressed as[18,19]

$$k_q = \chi(HPO_4^{2-})[\text{phosphate}]_T k_{PCET}^{bi} + k_{ET} \qquad (18)$$

where $[\text{phosphate}]_T$ is the total concentration of phosphate buffer and $\chi(HPO_4^{2-})$ is the mole fraction of HPO_4^{2-} (i.e., $\chi(HPO_4^{2-}) = [HPO_4^{2-}]/[\text{phosphate}]_T$). The mole fraction $\chi(HPO_4^{2-})$ can be calculated as a function of pH using the following expression:

$$\chi(HPO_4^{2-}) = (10^{pK_a - pH} + 1)^{-1} \qquad (19)$$

with $pK_a = 7.2$ for HPO_4^{2-}. According to eq 19, the mole fraction $\chi(HPO_4^{2-})$ increases smoothly from zero to unity as the pH increases in the region $4 < pH < 9$. In eq 18, k_{PCET}^{bi} is the bimolecular rate constant for the PCET reaction in which the proton is transferred to HPO_4^{2-}, and k_{ET} is the rate constant for an ET reaction that is followed by rapid PT to the solvent.[18]

The rate constants in eq 18 have been obtained from experimental measurements.[18,19] The ET rate constant was determined to be $k_{ET} = (1.0 \pm 0.2) \times 10^5\ s^{-1}$ from measurements at $4 < pH < 8$ in the absence of phosphate buffer. The bimolecular PCET rate constant was determined to be $k_{PCET}^{bi} = (1.7 \pm 0.1) \times 10^7\ M^{-1}\ s^{-1}$ from measurements of k_q as a function of phosphate buffer concentration at pH = 7.5, 8.3, and 9.2. The H/D KIE for the bimolecular PCET rate constant k_{PCET}^{bi} was determined to be ~3.0 from measurements of k_q as a function of phosphate buffer concentration at high pH for the reaction in H_2O and D_2O. For low pH, the reaction is dominated by ET, and the KIE of k_q should become closer to unity. The error associated with the experimental measurement of k_{ET} provides only a limiting value of KIE < 3.[18,19] For high pH, the KIE of k_q is the same as the KIE for k_{PCET}^{bi} at high phosphate buffer concentration (i.e., when the first term in eq 18 is dominant), but the KIE of k_q will become smaller at lower phosphate buffer concentration due to contributions from k_{ET}.

We calculated the overall rate k_q for hydrogen and deuterium transfer using the expression in eq 18, in conjunction with our PCET expression in eq 2. The experimental and calculated data are depicted in Figure 3. The proton donor−acceptor distance (i.e., the distance between the tyrosine oxygen and the phosphate oxygen) was determined to be 2.51 Å from the geometry optimization of the hydrogen-bonded complex in a dielectric continuum solvent, as described above. We used the experimentally determined $k_{ET} = (1.0 \pm 0.2) \times 10^5\ s^{-1}$ for all calculations. We fit the ET and PT couplings V^{ET} and V^{PT} in our model to reproduce the experimentally determined $k_{PCET}^{bi} = (1.7 \pm 0.1) \times 10^7\ M^{-1}\ s^{-1}$ and an H/D KIE of 3.0 for k_{PCET}^{bi}. The unimolecular PCET rate constant k_{PCET}^{uni}, given in eq 2, describes the PCET reaction in the hydrogen-bonded complex ReYOH- - -HPO_4^{2-}. In this model, the corresponding bimolecular rate constant k_{PCET}^{bi} measured experimentally is related to k_{PCET}^{uni} according to $k_{PCET}^{uni} = k_{PCET}^{bi}/K_{eq}$, where K_{eq} is the

(51) Gary, R.; Bates, R. G.; Robinson, R. A. *J. Phys. Chem.* **1964**, *68*, 3806−3809.

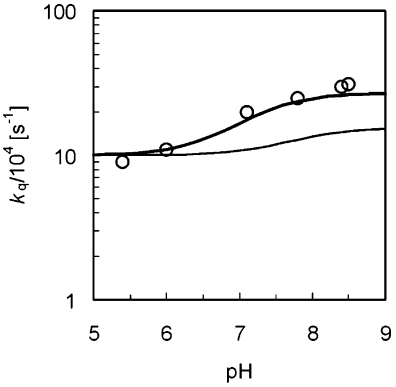

Figure 3. pH dependence of the overall rate constant k_q. The experimental data for k_q measured with 10 mM phosphate buffer in H_2O (Figure 3 in ref 9) are depicted with open circles (○). The rate constants for the phosphate-acceptor model with 10 mM phosphate buffer, calculated using eq 18, are depicted with thick and thin lines for the reaction in H_2O and D_2O, respectively. The rate constant for the reaction in H_2O or D_2O is plotted as a function of pH or pD, respectively, where the mole fraction $\chi(HPO_4^{2-})$ or $\chi(DPO_4^{2-})$ is calculated as a function of pH or pD using eq 19 with pK_a = 7.2 or 7.8, respectively.

Table 2. Analysis of k_{PCET}^{uni} for the Phosphate-Acceptor Model at 298 K with Phosphate Buffer Concentration of 10 mM

	R/P (μ/ν) state[a]			
	1/1	1/2	1/3	1/4
	Hydrogen			
contrib to rate (%)	3.3	8.8	67.8	1.6
$\Delta G°$ (kcal/mol)[b]	−21.15	−13.98	−11.17	−7.61
λ (kcal/mol)[c]	42.96	42.66	42.50	42.15
$\Delta G^{\dagger}$ (kcal/mol)[d]	2.77	4.82	5.77	7.08
V^2 [(kcal/mol)^2][e]	5.19×10^{-6}	4.38×10^{-4}	1.69×10^{-2}	3.54×10^{-3}
	Deuterium			
contrib to rate (%)	0.0	0.4	12.8	81.9
$\Delta G°$ (kcal/mol)[b]	−20.89	−15.59	−10.93	−9.92
λ (kcal/mol)[c]	43.03	42.87	42.53	42.18
$\Delta G^{\dagger}$ (kcal/mol)[d]	2.85	4.34	5.87	6.17
V^2 [(kcal/mol)^2][e]	3.49×10^{-8}	3.31×10^{-6}	1.25×10^{-3}	1.32×10^{-2}

[a] The R/P state refers to the indices of the reactant and product vibronic states. [b] Reaction free energy. [c] Total reorganization energy. [d] Activation free energy. [e] Squared non-adiabatic vibronic coupling.

equilibrium association constant to form the hydrogen-bonded complex. This equilibrium constant has been measured experimentally to be K_{eq} = 0.5 M^{-1} for tyrosine and HPO_4^{2-}.[52] For the KIE calculations, K_{eq} is assumed to be the same in H_2O and D_2O. For this model, with a total phosphate buffer concentration of 10 mM, the H/D KIE of k_q is ∼1.7 for relatively high pH and decreases to unity for low pH, where k_q is dominated by k_{ET}.

Analysis of the PCET calculations provides insight into the reorganization energies, reaction free energies, activation free energies, and vibronic couplings for the various pairs of reactant/product vibronic states for both hydrogen and deuterium transfer. These data are provided in Table 2 for the phosphate-acceptor model. Three reactant and five product vibronic states were included in the calculations, but only contributions from the ground reactant state are shown. The combined contributions from the excited reactant states are less significant because of the smaller Boltzmann probability for these states relative to the ground reactant state. Note that the total reorganization

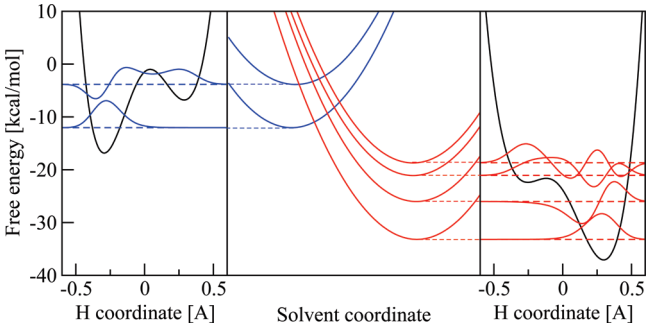

Figure 4. Analysis of the free energy surfaces for the PCET reaction in the phosphate-acceptor model for the ReYOH complex. In the center frame are slices of the two-dimensional ET diabatic free energy surfaces as functions of the solvent coordinates. The slices were obtained along the line connecting the minima of the lowest energy reactant (I) and product (II) two-dimensional free energy surfaces. In the left frame are the reactant (I) proton potential energy curve and the corresponding proton vibrational wave functions as functions of the proton coordinate evaluated at the minimum of the ground-state reactant free energy surface. In the right frame are the product (II) proton potential energy curve and the corresponding proton vibrational wave functions as functions of the proton coordinate evaluated at the minimum of the ground-state product free energy surface.

energies given in Table 2 include the contribution from the inner-sphere reorganization energy of 9.8 kcal/mol. The calculated outer-sphere (solvent) reorganization energy for the overall PCET reaction is ∼33 kcal/mol for all pairs of vibronic states. These solvent reorganization energies are not identical to the diabatic solvent reorganization energies in Table 1 because the terms in the rate expression involve mixtures of diabatic states (i.e., the reactant is a mixture of diabatic states 1*a* and 1*b*, and the product is a mixture of diabatic states 2*a* and 2*b*). The reorganization energies are sufficiently larger than the driving forces, indicating that the systems are in the normal Marcus region.

In the phosphate-acceptor model, the dominant contribution to the rate arises from nonadiabatic transitions between the ground reactant state and the third product state for hydrogen and the fourth product state for deuterium. These contributions exceed the contributions from the nonadiabatic transition between the ground reactant and product states because the larger vibronic coupling overrides the slightly higher activation free energy barrier. The larger vibronic coupling is due mainly to the greater overlap between the reactant and product proton vibrational wave functions. This effect is more pronounced for deuterium than for hydrogen. The free energy surfaces and the corresponding proton vibrational wave functions are depicted in Figure 4.

In the water-acceptor model, the proton is transferred directly to the bulk water. Our strategy was to fit the ET and PT couplings V^{ET} and V^{PT} in our model to reproduce the experimentally determined overall rate constant k_q at pH = 8.5 and 5.4. The proton donor−acceptor distance (i.e., the distance between the tyrosine oxygen and the water oxygen) was determined to be 2.67 Å from the geometry optimization of the hydrogen-bonded complex in a dielectric continuum solvent. This distance is larger than the proton donor−acceptor distance for the phosphate-acceptor model because the water molecule is neutral, whereas the phosphate molecule is negatively charged. Using the PCET rate expression in eq 2 in conjunction with this model, we were unable to reproduce both the experimentally measured pH dependence of k_q and the H/D KIE for parameters

(52) Alev-Behmoaras, T.; Toulme, J. J.; Helene, C. *Photochem. Photobiol.* **1979**, *30*, 533−539.

varied within physically reasonable ranges. These negative results suggest that the water-acceptor model as defined above is not physically reasonable for this system.

We conclude that the phosphate-acceptor model provides a better description of the PCET reaction in the ReYOH complex than the water-acceptor model. Experiments on other tyrosine oxidation systems[11] have also indicated that deprotonation of tyrosine in PCET reactions is controlled by the availability of suitable base from the buffer.

IV. Concluding Remarks

In this paper, we evaluated two different models for tyrosyl radical generation in the $[Re(P-Y)(phen)(CO)_3]PF_6$ system. In the phosphate-acceptor model, the phosphate buffer species HPO_4^{2-} serves as the proton acceptor, and the pH dependence of the overall rate arises from the titration between the HPO_4^{2-} and $H_2PO_4^-$ forms of the phosphate buffer. In the water-acceptor model, bulk water serves as the proton acceptor. Our calculations indicate that the phosphate-acceptor model can successfully reproduce the experimentally observed pH dependence of the overall rate and H/D KIE, whereas the water-acceptor model is not physically reasonable for this system. Analysis of the results suggests that the phosphate buffer species HPO_4^{2-} is favored over water as the proton acceptor in part because the proton donor−acceptor distance is ∼0.2 Å smaller for the phosphate acceptor due to its negative charge. This smaller proton donor−acceptor distance leads to a larger vibronic coupling because of the greater overlap between the reactant and product proton vibrational wave functions. Other factors differentiating these two mechanisms include the slightly smaller outer-sphere reorganization energy for PCET in the phosphate-acceptor model and the differences in driving forces for PCET.

Within the phosphate-acceptor model, we analyzed the physical quantities impacting the overall rate constant, including the reorganization energies, reaction free energies, activation free energies, and vibronic couplings for each pair of reactant/product vibronic states. We calculated the outer-sphere reorganization energy for the overall PCET reaction to be ∼33 kcal/mol for all pairs of vibronic states. Moreover, the dominant contribution to the rate arises from nonadiabatic transitions between the ground reactant state and the third product state for hydrogen transfer and the fourth product state for deuterium transfer. These contributions dominate over contributions from lower product states because of the larger vibronic coupling, which arises from the greater overlap between the reactant and product proton vibrational wave functions.

These calculations provide insight into the fundamental mechanism of tyrosyl radical generation. Such insights have implications for a broad range of biologically important processes. For example, the conclusion that the phosphate serves as a proton acceptor is consistent with experimental observations in D1-His190 mutants of PSII, where the rates of $P680^{+\bullet}$ reduction by Y_z increased dramatically in the presence of imidazole and other small organic bases.[53,54] Thus, these types of calculations on model systems can play a significant role in elucidating the mechanisms of complex biological processes.

Acknowledgment. We are grateful to Steve Reece and Dan Nocera for sharing their experimental data prior to publication and for valuable discussions. Steve Reece's comments and insights were essential to this work. We are also grateful to Elizabeth Hatcher for helpful discussions. This work was supported by NSF grant CHE-05-01260 and was sponsored in part by the Division of Chemical Sciences, Geosciences, and Biosciences, Office of Basic Energy Sciences, U.S. Department of Energy, under contract from Oak Ridge National Laboratory.

Supporting Information Available: Atomic coordinates and partial charges used for the solvent reorganization energy calculations; total energy of the optimized ReYOH structure; complete ref 35; figure illustrating the sensitivity of the KIE for the phosphate-acceptor model to the coupling parameter V^{PT} and the inner-sphere reorganization energy λ_{in}. This material is available free of charge via the Internet at http://pubs.acs.org.

JA072708K

(53) Hays, A.-M. A.; Vassiliev, I. R.; Golbeck, J. H.; Debus, R. J. *Biochemistry* **1998**, *37*, 11352−11365.
(54) Hays, A.-M. A.; Vassiliev, I. R.; Golbeck, J. H.; Debus, R. J. *Biochemistry* **1999**, *38*, 11851−11865.